Rare Metal Materials and Engineering
Volume 53, Issue 3, March 2024
Available online at www.rmme.ac.cn

Science Press

Cite this article as: Guo Jialiang, Wang Fang, Liou Juin J, et al. Parallel Groove-Textured TB6 Titanium Alloy Surfaces for Improving Wettability, Tribological Properties and Corrosion Resistance[J]. Rare Metal Materials and Engineering, 2024, 53(03): 617-624. DOI: 10.12442/j.issn.1002-185X.20230268.

ARTICLE

Parallel Groove-Textured TB6 Titanium Alloy Surfaces for Improving Wettability, Tribological Properties and Corrosion Resistance

Guo Jialiang[1], Wang Fang[1,2,3,4], Liou Juin J[5], Liu Yuhuai[1,2,3,4]

[1] International Joint-Laboratory of Electronic Materials and Systems of Henan Province, National Center for International Joint Research of Electronic Materials and Systems, School of Electrical and Information Engineering, Zhengzhou University, Zhengzhou 450001, China; [2] Institute of Intelligence Sensing, Zhengzhou University, Zhengzhou 450001, China; [3] Research Institute of Industrial Technology Co., Ltd, Zhengzhou University, Zhengzhou 450001, China; [4] Zhengzhou Way Do Electronics Co., Ltd, Zhengzhou 450001, China; [5] School of Electrical and Information Engineering, North Minzu University, Yinchuan 750001, China

Abstract: We proposed an efficient method to fabricate superhydrophobic, wear and corrosion resistant groove-textured surfaces based on TB6 (Ti-10V-2Fe-3Al) titanium alloy substrates. The smooth surface of the titanium alloy was ablated using a nanosecond laser to create a surface with a parallel groove pattern. In order to further improve the surface hydrophobicity, the laser treated surface was irradiated by an ultraviolet lamp for 1 h and subsequently immersed in a 3wt% octadecyltrichlorosilane solution for 2 h for chemical modification. The wettability of the groove-textured surfaces with varying groove spacing was investigated by analyzing surface morphology and chemical composition. Results show that the average coefficient of friction (COF) of the superhydrophobic surface is reduced by 34%, 56%, and 59% compared with that of the original hydrophilic surface under dry, water, and oil lubrication conditions, respectively. The mechanism variation of the CoF was also discussed. Potentiokinetic polarization testing demonstrates that the prepared superhydrophobic surface provides corrosion protection for the titanium alloy substrate.

Key words: laser texturing; titanium alloy; superhydrophobicity; tribological properties; corrosion resistance

Titanium and its alloys have been extensively utilized in multiple industries, primarily due to their exceptional mechanical properties, corrosion resistance, and biocompatibility[1–2]. However, despite their remarkable characteristics, titanium alloys suffer from wear and corrosion issues, especially under severe working conditions, such as high loads, high temperatures, and corrosive environments, which restrain their widespread application in engineering[3]. To overcome these limitations, various surface modification techniques such as coating, ion implantation and thermal spraying have been developed to enhance the tribological performance of titanium alloys[4]. Despite their effectiveness, these methods are not infallible. Surface coatings can delaminate or degrade under mechanical stress[5], while the surface strengthening layer produced by ion implantation technology is usually thin (less than 1 μm) due to limitations in ion implantation energy[6]. In addition, the thermal spraying modified layer has a loose microstructure, and its bonding strength with the substrate is relatively low, which makes it challenging to form a metallurgical bond with high bonding strength[7]. Laser texturing, which involves the use of a high-energy laser beam to produce micro/nano structures on a material surface, has become a controllable, cost-effective, and environmentally friendly technique for altering surface properties of the material[8]. Shen et al[9] reported superhydrophobic TC4 (Ti-6Al-4V) titanium alloy surfaces in color, including blue,

Received date: May 06, 2023
Foundation item: National Natural Science Foundation of China (62174148); National Key Research and Development Program (2022YFE0112000, 2016YFE0118400); Key Program for International Joint Research of Henan Province (231111520300); Ningbo Major Project of "Science, Technology and Innovation 2025" (2019B10129); Zhengzhou 1125 Innovation Project (ZZ2018-45)
Corresponding author: Liu Yuhuai, Ph. D., Professor, International Joint-Laboratory of Electronic Materials and Systems of Henan Province, National Center for International Joint Research of Electronic Materials and Systems, School of Electrical and Information Engineering, Zhengzhou University, Zhengzhou 450001, P. R. China, Tel: 0086-371-67781540, E-mail: ieyhliu@zzu.edu.cn

yellow and tan, which was achieved by inducing various micro/nano structures on the titanium alloy surface using femtosecond laser illumination with different tilt angle incidences. Yu et al[10] used orthogonal experiments to investigate the influence of picosecond laser processing parameters on the morphology of induced microstructure of the TC4 titanium alloy surface, and successfully fabricated titanium alloy for biological implantation which can improve the adhesion and proliferation of osteoblasts by optimized process parameters. Liu et al[11] produced cell-like patterns on the TC4 titanium alloy by nanosecond laser surface texturing technique and demonstrated the ability of the modified surface to reduce the coefficient of friction (COF) by 32.4% in a simulated body fluid environment. The above works all selected TC4 titanium alloy as the substrate material. TB6 (Ti-10V-2Fe-3Al) titanium alloy, a type of proximal beta-titanium alloy, is mainly driven by the objective of weight-saving in aerospace applications, as it can achieve a mass reduction up to 30% compared with TC4 components at the same strength level, which is a critical factor in maintaining structural efficiency and remaining competitive advantage in the airframe market, particularly in the current scenario of increasing fuel costs[12]. Most of the current research on TB6 titanium alloy focuses on the tensile deformation behavior[13], fatigue behavior[14], and electrochemical behavior[15]. However, to the best of our knowledge, there is a lack of investigation regarding the tribological properties of superhydrophobic TB6 titanium alloy surfaces. In order to fill the current research gap, this study sought to fabricate parallel grooves on the TB6 titanium alloy surface by ablating with an ultraviolet (UV) nanosecond laser, and the laser treated surface was chemically treated by immersion in octadecyltrichlorosilane (OTS) solution to obtain a superhydrophobic surface.

The morphology of the micro/nano structure and the chemical composition of the sample surface were observed by confocal microscopy and scanning electron microscopy (SEM). The effect of the linear spacing of parallel grooves on the wettability and tribological properties of textured titanium alloy surfaces was studied. The proposed method in this study offers the advantages of cost effectiveness, high efficiency, good reproducibility, and easy operation. Moreover, it is expected to provide a theoretical basis for the large-scale production of superhydrophobic wear-resistant and corrosion-resistant TB6 titanium alloy workpieces.

1 Experiment

The substrate material was a TB6 titanium alloy sheet with dimensions of 30 mm×30 mm×3 mm, which was subsequently ground with 400, 600, and 800 mesh sandpaper sequentially until a surface roughness (S_a, arithmetic mean height) of less than 0.2 μm was attained. To remove surface contaminants before the surface modification steps, the substrates were subjected to sequential ultrasonic cleaning with petroleum ether, anhydrous ethanol, and deionized water for 2 min each time. After the aforementioned step, ablation of the substrates was performed by parallel line-by-line scanning with a self-made laser processing system. As shown in Fig.1, a UV nanosecond pulsed laser (AWAVE 355-10-50-W, Advanced Optowave, USA) was used as a light source part of the laser processing system to ablate and to pattern titanium alloy surfaces. The laser was operated at a central wavelength of 355 nm, a power output of 10 W, and a pulse width of 11 ns. Additionally, the system was equipped with an F-θ lens that had a focal length of 255 mm and was capable of projecting a spot with approximately 60 μm in diameter onto the sample. The repetition rate, scanning speed, and scanning cycles of the laser process were configured to 40 kHz, 500 mm/s, and 15, respectively, to fabricate patterned surfaces with distinctive densities of parallel line patterns. To achieve this, the laser scanning intervals (i.e., the groove spacing) of 50, 100, 150, 200, 250, 300, 350, and 400 μm were selected. The laser treated titanium alloy samples were positioned about 10 cm from a UV lamp emitting light with a center wavelength of 365 nm and a power output of 250 W, and they were continuously irradiated for 1 h to induce surface hydroxylation. The next step was immersing the samples in 3wt% OTS solution for 2 h to carry out chemical surface modification. Subsequently, the samples underwent ultrasonic cleaning by petroleum ether, anhydrous ethanol, and deionized water for 2 min. Finally, a pet hair dryer (CS-2400, CHUNZHOU, China) was employed to fully dry the samples, thereby completing the sample fabrication process.

Confocal laser microscope (LEXT OLS5100, Olympus, Japan) was employed for surveying and calculating the surface three-dimensional morphologies and S_a, while SEM (Verios 5 UC, Thermo Fisher Scientific, USA) was used to observe the two-dimensional morphologies of the sample surface. Furthermore, energy dispersive spectrometry (EDS, UltimMax100, Oxford Instruments, England) was employed to analyze the content of various chemical elements on the sample surface. Automated capture on the contour of 3 μL droplets of deionized water was accomplished using an optical contact angle meter (OCA25, DataPhysics, Germany). The

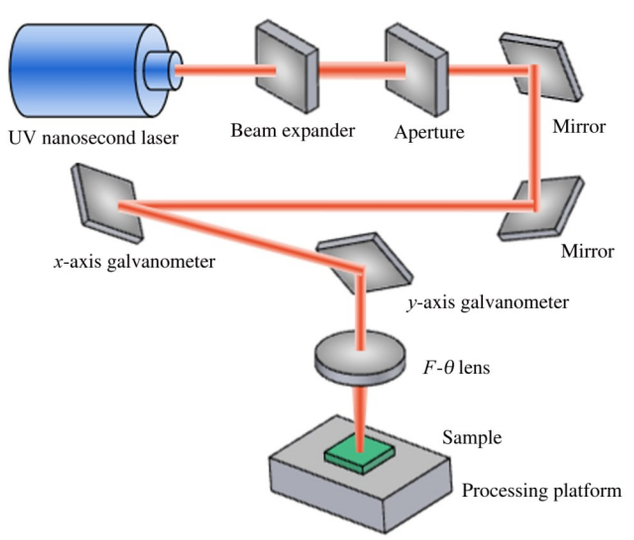

Fig.1 Schematic diagram of UV nanosecond laser processing system

static water contact angle (WCA) of the sample surface was subsequently calculated using software specifically designed for the equipment. The measurement of WCA at five different locations on various surfaces was conducted to assess the surface wettability. The instantaneous COF of the sample surface during sliding reciprocating tests was monitored using a ball-on-flat type linear reciprocating tribotester (UMT-5, Bruker, USA) under three different conditions: dry friction, deionized water, and oil lubrication. The EasyCheer® ATF6, a fully synthetic automatic transmission fluid, was used as the lubricant for oil lubrication, which had a kinematic viscosity of 27.47 and a viscosity index of 157 at 25 °C. The sliding reciprocating test used the Si_3N_4 ball with 10 mm in diameter as the sliding pair. The samples were held still while the sliding pairs underwent reciprocating sliding under a load of 1 N for 600 s, a sliding amplitude of 6 mm, and a frequency of 1 Hz. The average COF during sliding was determined after conducting three tests on each surface with different texture patterns and sliding conditions, ensuring statistical significance. A potentiostat (Reference 600, Gamry Instruments, USA) was used to conduct electrochemical corrosion tests in a 3.5wt% NaCl aqueous solution at room temperature. The potentiodynamic polarization curve was recorded using a three-electrode system consisting of the tested sample as the working electrode, a platinum sheet with dimensions of 10 mm×10 mm×0.1 mm as the counter electrode, and a saturated calomel electrode as the reference electrode.

2 Results and Discussion

2.1 Surface morphology and chemical state

The TB6 titanium alloy surface was exposed to a moving laser beam with a high spot overlapping percentage, which led to the heating, melting, and evaporation of metal from its surface[16], thus creating parallel micro-groove structures. Fig.2 shows the cross-sectional profile of the individual groove texture along with its three-dimensional morphology, which reveals the existence of bulge structures at the edges of the micro-grooves due to the material accumulation during the laser ablation process. For individual groove texture, the groove inner diameter was defined as the width of the part indented to the original smooth surface, whereas the outer diameter of the groove was obtained by adding the width of the bulge structure on both sides of the groove to the groove inner diameter. The dimensions of individual groove texture were approximately 25 μm in inner diameter, 50 μm in outer diameter, 17 μm in height, and 20 μm in depth.

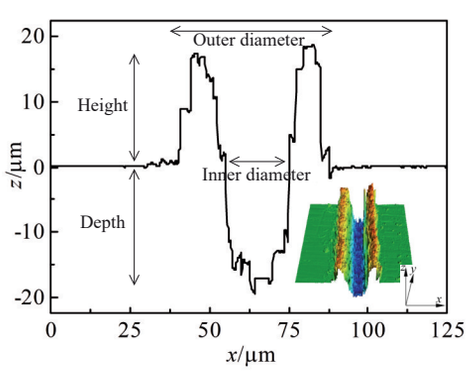

Fig.2 Cross-sectional profile and three-dimensional morphology of individual groove texture

Fig. 3 shows the SEM and EDS results of the patterned surface (groove spacing=100 μm), revealing that the titanium alloy surface is patterned with parallel grooves featuring bulge structures. Additionally, the spattering of the removed material results in random distribution of particle structures on the surface. A micro-nano hierarchical surface is synergistically constructed by micro-groove, bulge, and particle structure. Successful formation of OTS film on the groove-textured surface is suggested by the appearance of silicon (Si) element and an increase in carbon (C) and oxygen (O) elements on the chemically treated surface, compared with the untreated textured surface. While the surface morphology of the groove-textured surface has minimal changes after immersion in OTS solution, and the number of micro-particles on its surface significantly increases. This is attributed to the successful self-assembly of the OTS film, especially the clustering of certain OTS molecules on the surface, resulting in the formation of siloxane dots.

2.2 Surface wettability

The quantification of wettability, which describes the ability of a liquid to spread on a solid surface, is typically based on the value of the WCA. A solid surface is classified as hydrophilic or hydrophobic based on whether its WCA is less than or greater than 90°, and surfaces exhibiting WCAs greater than 150° are considered as superhydrophobic ones[17].

The Young equation[18] is shown as follows:

$$\cos\theta = \frac{\gamma_{sv} - \gamma_{sl}}{\gamma_{lv}} \quad (1)$$

where θ refers to the specific WCA on the solid surface, which is defined as the angle formed by the tangent line at the three-phase interface and the edge of the water droplet; γ_{lv}, γ_{sv}, and γ_{sl} represent the surface energies of the liquid-gas, solid-gas, and solid-liquid interfaces, respectively. The wettability of a material is affected by its surface energy: low surface energy impedes wetting by water droplets while high surface energy promotes spontaneous wetting and makes it easy for wetting by water droplets. The smooth surface samples before and after chemical modification are labeled as S1 and S2, respedtively, while the groove-textured surface samples (groove spacing=100 μm) before and after chemical modification are labeled as S3 and S4, respectively. As shown in Fig. 4, the original smooth surface (S1) exhibits hydrophilicity with a WCA of 82°, whereas the original surface treated with OTS solution (S2) shows hydrophobicity with a WCA of 110°, indicating that OTS molecules can reduce the free energy of the surface. Sequential treatment of the surface with laser and UV radiation (S3) generates abundant high free energy hydroxyl groups on the surface, resulting in superhydrophilicity with a WCA close to 0°. Moreover, when the groove-textured surface is immersed in

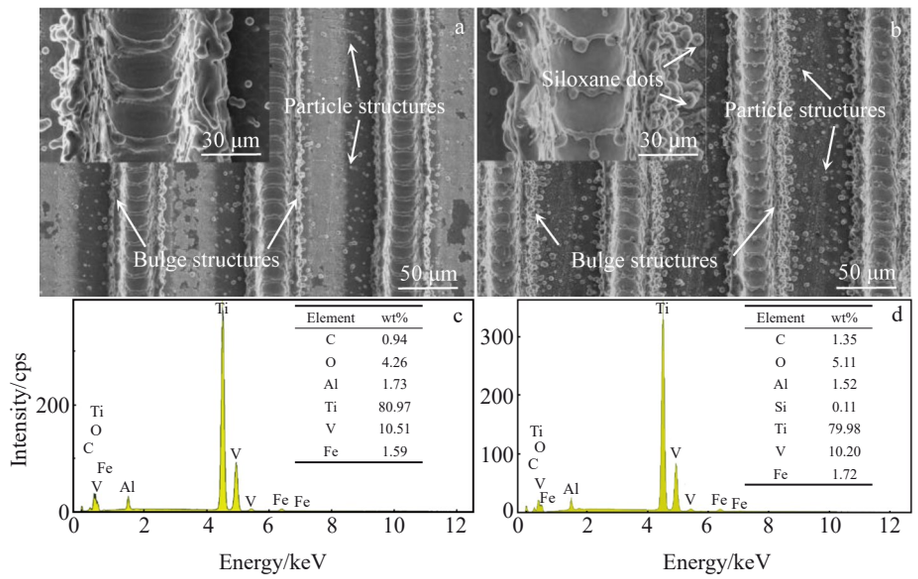

Fig.3 SEM images (a–b) and EDS results (c–d) of untreated (a, c) and chemically treated (b, d) groove-textured titanium alloy surfaces with a groove spacing of 100 μm

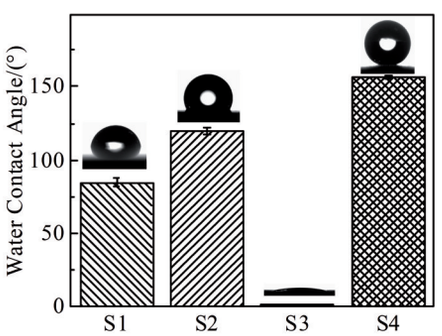

Fig.4 Water contact angles on TB6 titanium alloy substrate (S1), chemically treated substrate (S2), groove-textured substrate (S3) and superhydrophobic samples (S4)

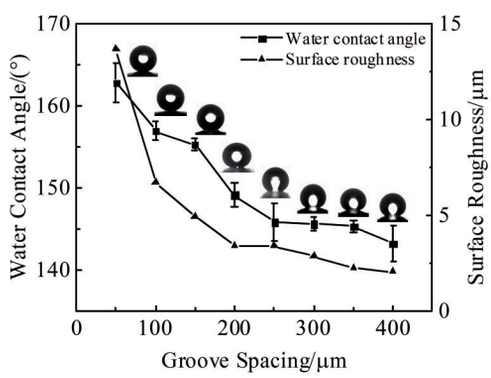

Fig.5 Variation in the water contact angle and surface roughness of the textured TB6 titanium alloy surface with different groove spacings

OTS solution (S4), dehydration condensation reaction occurs between the hydroxyl groups and OTS molecules, leading to the self-assembly of low free energy OTS molecules on the surface, resulting in superhydrophobic surface.

The effect of groove spacing on the wettability of titanium alloy with parallel groove texture is shown in Fig. 5. With the increase in the groove spacing of the texture from 50 μm to 400 μm, a consistent reduction from 162.8° ±2.4° to 143.2° ±2.2° in the WCA can be observed. This trend is aligned with the changes in S_a within the same spacing range from 13.6 to 2.1, implying that a smoother surface is associated with both lower WCA and S_a. At groove spacings of 50, 100, and 150 μm, the patterned surface exhibits WCAs of 162.8°±2.4°, 157° ±1.2°, and 155.2°±0.7°, respectively. However, superhydrophilicity is no longer observed on the groove-textured surface when the groove spacing is ≥200 μm.

The surface wettability relationship of inhomogeneous surfaces proposed by Cassie and Baxter[19] is as follows:

$$\cos\theta_r = f_1 \cos\theta - f_2 \quad (2)$$

where f_1 and f_2 correspond to the ratios of solid-liquid and air-liquid interfacial areas with $f_1+f_2=1$ respectively; θ_r and θ correspond to the WCA on textured and smooth titanium alloy surface, respectively. The smooth surface is roughened by the presence of micro-grooves on its surface. Dense grooves on the surface tend to trap more air in the spaces between the droplets and the rough structures, which creates air pockets to prevent water from contacting with the material surface. However, increasing the groove spacing results in sparser grooves and reduces S_a, which decreases the solid-liquid area of contact and provides greater accessibility of droplets to the groove interior, resulting in a decrease in WCA.

2.3 Tribological behavior

Fig. 6 shows the average COF of smooth and groove-textured surfaces in contact with Si_3N_4 ball after sliding under dry friction, water lubrication, and oil lubrication conditions for 600 s. The original smooth surface (groove spacing=0 μm) shows inferior wear resistance with an average COF of 0.537

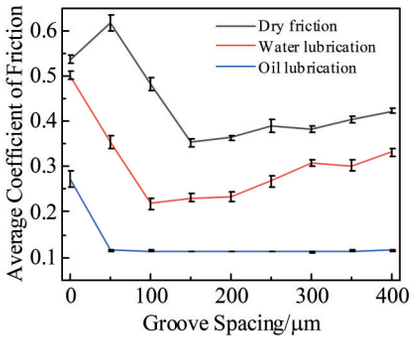

Fig.6 Average coefficient of friction of the original surface, and groove-textured surface with different groove spacings under dry, water, and oil lubrication conditions

under dry friction, while the average COF of the groove-textured surface decreases initially and then increases with increasing groove spacing. When parallel grooves with 50 μm in intervals are textured onto the titanium alloy surface, the surface becomes covered with densely packed grooves featuring bulge structures. This results in a higher average COF of 0.617 compared with the original surface. The underlying reasons for this will be explained below. The limited actual contact area between the friction pairs generates significant contact stress, which causes plastic deformation of the friction pair contact surface[20]. During sliding, the friction pairs continually ground against each other. The groove-textured surface experiences a higher average contact stress, which causes stress concentration at the boundary of the micro-grooves. Consequently, micro-cracks initiate and are propagated at the point with stress concentration, leading to the deformation and fracture of the micro-grooves. In addition, the presence of micro-grooves increases the roughness of the titanium alloy surface, and excessive micro-grooves significantly increase the resistance to relative motion between the friction pairs[21]. With a groove spacing of 100 μm or more, the average COF is lower than that of the original surface. This improvement can be attributed to the effective capture of wear debris by the micro-grooves[22], which prevent wear debris from cutting the titanium alloy surface, thereby inhibiting the three-body wear mechanism and reducing ploughing. Increasing the groove spacing from 150 μm to 400 μm leads to a decrease in the number of micro-grooves on the titanium alloy surface. This increases the actual contact area of the friction pair, resulting in a stronger adhesion effect[23]. Additionally, the decrease in the number of micro-grooves suggests that some wear debris are unable to be captured in time, leading to a gradual increase in the average COF from its lowest point of 0.354 to 0.424.

Under water lubrication conditions, the original surface shows a lower average COF of 0.502 compared with that under dry friction. The decrease in COF can be attributed to the water's ability to effectively clear wear debris during sliding and to reduce shear strength between the Si_3N_4 ball and the titanium alloy surface[24]. A similar trend under dry friction conditions is also observed in the average COF of groove-textured surfaces under water sliding environment with a gradual decrease followed by an increase as the groove spacing increases from 50 μm to 400 μm. However, the average COF of all the groove-textured surfaces under water lubrication is found to be lower than that of the original surface under dry friction condition. Further, groove-textured surfaces with identical groove spacing under water lubrication show an average COF of 0.1–0.3, lower than that under dry friction condition. The JKR model[25] states that the hydrophobic surface with low free energy lowers the adhesion in the normal direction of the contact surface, resulting in a subsequent decrease in COF. The minimum average COF under water lubrication is obtained at a groove spacing of 100 μm, which is 0.219.

When sliding with oil as the lubricant, the original surface shows an average COF of 0.26, indicating that the oil has good anti-wear and lubrication properties. Meanwhile, the groove-textured surface exhibits a more stable and effective anti-friction effect, and all tested patterned surfaces have a COF of approximately 0.113. The average COFs all reach a minimum of 0.112 when the groove spacing is set as 200, 250, and 300 μm. Surface micro-grooves serve as effective reservoirs for lubricant storage, and each micro-groove can function as a hydrodynamic bearing[26]. The flow space of the lubricant on the titanium alloy surface changes in a "narrow-wide-narrow" pattern along a U-shaped groove section profile, generating pressure fluctuations and resulting in a pressure difference. Pressure flow and shear flow on the titanium alloy surface facilitate the formation of a stable load-bearing lubricating oil film, providing additional load-bearing capacity and secondary lubrication and leading to a reduced COF. The micro-texture on the surface stores oil and wear debris to prevent three-body wear and to reduce ploughing. Groove-textured surfaces with groove spacings ranging from 50 μm to 400 μm provide favorable conditions for the formation of continuous oil films. As a result, under dry, water, and oil lubrications, the groove-textured surfaces demonstrate a significant reduction in COF of 34%, 56%, and 59% compared with the original surface, respectively.

Fig.7a shows the evolution of COF over a sliding time of 0 s to 600 s for the original surface under various sliding conditions. The COF of the original surface is found to surge to more than 0.4 after only 10 s of sliding initiation against Si_3N_4 balls in all tested conditions due to its poor wear resistance. During the first 300 s of sliding time, the COF shows a similar random fluctuation between 0.45 and 0.6 under both dry friction and water lubrication. After that, the sample under dry friction experiences a slow upward trend in fluctuation due to continuous wear with instantaneous COF even exceeding 0.6 at approximately 550 s. In contrast, the sample under water lubrication is benefited from flushing and reduced shear strength, which enables it to maintain a COF of approximately 0.52 even after nearly 600 s of sliding. During the entire test duration of 0–600 s, the COF of the samples under oil lubrication condition shows a fluctuating decreasing

trend within the range of 0.2−0.4. However, the amplitude of these fluctuations is significantly larger than that of the samples tested under dry friction and water lubrication conditions. This is because it is challenging to establish an efficient oil film between the friction pairs, resulting in the contact surfaces being in a state of boundary lubrication[27].

Fig. 7b shows how the COF changes over time for the groove-textured surface (groove spacing=100 μm) subjected to various sliding conditions within 0−600 s. Benefiting from the smaller actual contact area between the friction pairs, the adhesion effect is weakened, leading to a significantly slower rise in COF within seconds after the start of sliding, compared with the original surface. The COF continues to increase under dry friction condition for 50 s and water lubrication condition for 100 s, as the Si_3N_4 ball is preferentially in contact with the bulge structures of the patterned surface during early sliding, in which the COF increases from 0 to about 0.5 and 0.4, respectively. Subsequently, the capture effect of wear debris causes a gradual reduction in COF. The COF under dry friction condition shows a gradual increase after 200 s, as the textured surface further wears under dry friction condition, and thus wear debris is accumulated and filled in the micro-grooves. Finally, after almost 600 s, the COF reaches a level similar to that of the original surface with a value of approximately 0.53. In addition, water lubrication condition maintains a constant COF of about 0.19 after sliding for 250 s, due to the extreme hydrophobicity of surface, which enables water to flow easily from the titanium alloy surface to the Si_3N_4 ball, creating a water film that improves lubrication[28]. However, the higher viscosity of oil, higher than that of water, allows for the formation of a stable lubricating film, leading to a stable COF of approximately 0.114 for the entire 600 s of the siding test.

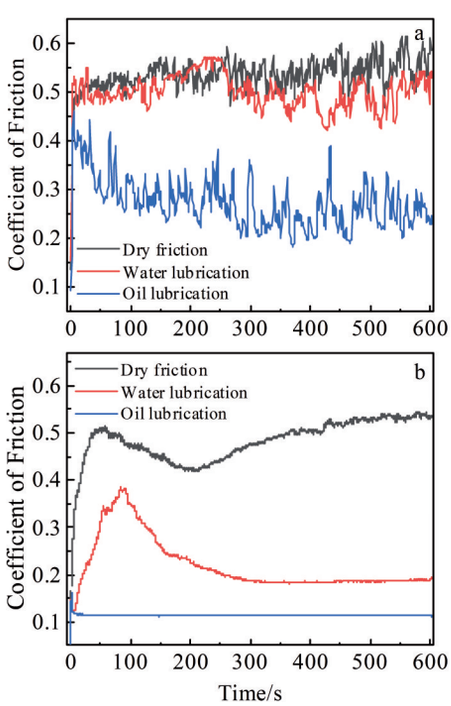

Fig.7 Variation in coefficient of friction with sliding time under dry friction, water and oil lubrications: (a) original surface and (b) groove-textured surface (groove spacing=100 μm)

2.4 Corrosion resistance

Fig. 8 shows the potentiodynamic polarization curves of various titanium alloy surfaces in 3.5wt% NaCl solution. The corrosion potential (E_{corr}) of these surfaces and the values of corrosion current density (I_{corr}) calculated based on Tafel extrapolation method are shown in Table 1. As a rule, a higher E_{corr} or lower I_{corr} observed from the polarization curve indicates a better corrosion resistance or lower corrosion rate. The surface of the titanium alloy textured only by laser (S2) shows improved corrosion performance with E_{corr} of −216 mV and I_{corr} of 250 nA·cm^{-2}, compared with the original surface (S3) with E_{corr} of −367 mV and I_{corr} of 628 nA·cm^{-2}. This is possibly attributed to the compact oxide film formed on the titanium alloy surface during laser processing[29], which retards the corrosion reaction process and suppresses the unrestricted diffusion and transfer of oxygen-containing ions and free electrons at the interface between the titanium alloy and the dielectric solution. After chemical modification of the surface (S2), a positive shift of E_{corr} and a decrease in I_{corr} are observed, suggesting the presence of corrosion resistance from the OTS film. However, the superhydrophobic surface (S4) exhibits the highest corrosion resistance with the most positive E_{corr} of −54 mV and the lowest I_{corr} of 205 nA·cm^{-2}. The hierarchical rough microstructures with gaps presenting on superhydrophobic surfaces make it challenging for corrosive chloride ions and

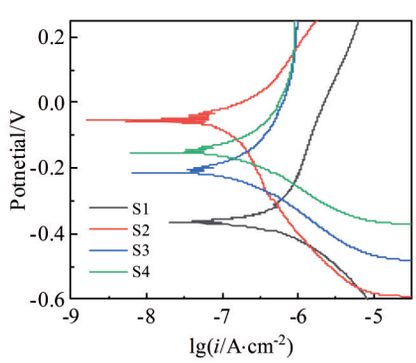

Fig.8 Potentiodynamic polarization curves of TB6 titanium alloy substrate (S1), chemically treated substrate (S2), laser textured substrate (S3) and superhydrophobic samples (S4) in 3.5wt% NaCl solution

Table 1 Corrosion potential (E_{corr}) and corrosion current density (I_{corr}) values of various samples

Sample	E_{corr}/mV	I_{corr}/nA·cm^{-2}
S1	–367	628
S2	–154	272
S3	–216	250
S4	–54	205

water to penetrate into them[30]. As a result, a large amount of air is entrapped between the liquid and solid interfaces, thereby reducing the contact area between the corrosive solution and the sample surface, which enhances corrosion resistance.

3 Conclusions

1) Laser ablation is employed to fabricate a patterned surface on TB6 titanium alloy substrate, which is featured by parallel micro-groove structures. The thermal and splash effects engender the formation of bulge and small particle structures, which, in conjunction with the micro-grooves, culminate in a micro/nano hierarchical surface. Subsequent chemical treatment facilitates the formation of octadecyltrichlorosilane (OTS) points on the groove-textured surface, thereby enhancing the density of surface particle structures.

2) Increasing the groove spacing on the groove-textured surface results in a decrease in both water contact angle (WCA) and surface ronghness (S_a). The maximum WCA of 162.8° ±2.4° and S_a of 13.6 can be obtained at a groove spacing of 50 μm.

3) The capture of wear debris and limited actual contact area between the friction pairs are the main factors that reduce coefficient of friction (COF) of groove-textured surfaces under unlubrication friction. Moreover, the low free energy of the chemically treated surface facilitates a further reduction in COF under water lubrication conditions. With the assistance of the hydrodynamic effect, all prepared groove-textured surfaces show very low COF under oil lubrication. The prepared superhydrophobic surface exhibits an average COF reduction of 34%, 56%, and 59% under dry, water, and oil lubrication conditions compared with the original hydrophilic surface, respectively.

4) Laser texturing and chemical modification are beneficial to enhance the corrosion resistance of titanium alloys, and the superhydrophobic surface exhibits the utmost resistance. The increase in E_{corr} of the superhydrophobic surface from −367 mV to −54 mV and the decrease in I_{corr} from 628 nA·cm^{-2} to 205 nA·cm^{-2}, compared with those of the original surface, validate the improved corrosion resistance.

References

1 Cui C, Hu B M, Zhao L *et al*. *Materials & Design*[J], 2011, 32(3): 1684

2 Diao Guilin, Sun Xuetong, Lin Huaishu *et al*. *Rare Metal Materials and Engineering*[J], 2021, 50(6): 2144 (in Chinese)

3 Siony N, Vuong L, Lundaajamts O *et al. Materials Today Communications*[J], 2022, 33: 104465

4 Uwais Z A, Hussein M A, Samad M A *et al. Arabian Journal for Science and Engineering*[J], 2017, 42: 4493

5 Huang Feng, Nie Ming, Lin Jiedong *et al. Rare Metal Materials and Engineering*[J], 2017, 46(12): 3693

6 Wei R. *Surface and Coatings Technology*[J], 1996, 83(1 – 3): 218

7 Sahoo B, Das T, Paul J. *Surface Review and Letters*[J], 2022, 29(9): 1

8 Mao B, Siddaiah A, Liao Y *et al. Journal of Manufacturing Processes*[J], 2020, 53: 153

9 Shen X, Yang L, Fan S *et al. Optics Communications*[J], 2020, 466: 125687

10 Yu Z, Yang G, Zhang W *et al. Journal of Materials Processing Technology*[J], 2018, 255: 129

11 Liu Q, Liu Y, Li X *et al. Wear*[J], 2021, 477: 203784

12 Boyer R R. *JOM*[J], 1980, 32(3): 61

13 Ma X, Li F, Cao J *et al. Materials Science and Engineering A*[J], 2018, 710: 1

14 Yao C F, Tan L, Ren J X *et al. Journal of Failure Analysis and Prevention*[J], 2014, 14: 102

15 Tang J, Luo H, Qi Y *et al. Electrochimica Acta*[J], 2018, 283: 1300

16 Misyura S Y, Kuznetsov G V, Feoktistov D V *et al. Surface and Coatings Technology*[J], 2019, 375: 458

17 Barthwal S, Barthwal S. *Journal of Applied Polymer Science*[J], 2023: 140(17): e53766

18 Adam N K. *Nature*[J], 1957, 180(4590): 809

19 Cassie A B D, Baxter S. *Transactions of the Faraday Society*[J], 1944, 40: 546

20 Guo J, Wang F, Liou J J *et al. Ukrainian Journal of Physical Optics*[J], 2022, 23(4): 243

21 Li Dan, Yang Xuefeng, Lu Chongyang *et al. Tribology International*[J], 2020, 142: 106016

22 Wang C, Li Z, Zhao H *et al. Tribology International*[J], 2020, 152: 106475

23 Rosenkranz A, Reinert L, Gachot C *et al. Wear*[J], 2014, 318(1–2): 49

24 Zhong Y J, Xie G Y, Sui G X *et al. Journal of Applied Polymer Science*[J], 2011, 119(3): 1711

25 Olah A, Hillborg H, Vancso G J. *Applied Surface Science*[J], 2005, 239(3–4): 410

26 Vermeulen M, Scheers J. *International Journal of Machine Tools and Manufacture*[J], 2001, 41(13–14): 1941

27 Chen G, Zhao J, Chen K *et al. Langmuir*[J], 2020, 36(4): 852

28 Chen D, Liu X, Zhang H *et al. Micromachines*[J], 2017, 8(7): 223

29 Chan C W, Lee S, Smith G *et al. Applied Surface Science*[J], 2016, 367: 80

30 Zhang B, Li J, Zhao X *et al. Chemical Engineering Journal*[J], 2016, 306: 441

平行沟槽织构对TB6钛合金表面润湿性、摩擦学性能和耐腐蚀性的改善

郭嘉梁[1]，王　芳[1,2,3,4]，刘俊杰[5]，刘玉怀[1,2,3,4]

(1. 郑州大学 电气与信息工程学院 电子材料与系统国际联合研究中心 河南省电子材料与系统国际联合实验室，河南 郑州 450001)

(2. 郑州大学 智能传感研究院，河南 郑州 450001)

(3. 郑州大学 产业技术研究院有限公司，河南 郑州 450001)

(4. 郑州唯独电子科技有限公司，河南 郑州 450001)

(5. 北方民族大学 电气与信息工程学院，宁夏 银川 750001)

摘　要：提出了一种快速制备具有超疏水性、耐磨性和耐腐蚀性的Ti-10V-2Fe-3Al（TB6）钛合金表面的方法。通过纳秒激光器对抛光的钛合金进行精确烧蚀，构筑了具有平行微沟槽阵列特征的织构表面。随后，利用紫外线灯照射和十八烷基三氯硅烷溶液浸渍进行化学改性，进一步增强了表面的疏水性。从表面形态和化学组分的角度分析了微沟槽间隔对织构表面润湿性的影响。结果表明，在干滑动、水润滑和油润滑条件下，所制备的超疏水表面相较于原始亲水表面，平均摩擦系数分别降低了34%、56%和59%。此外，分析了相关摩擦系数变化的机理。通过动电位极化测试验证，所制备的超疏水表面展现出优异的耐腐蚀性，为钛合金基体提供了有效的长期保护。

关键词：激光织构；钛合金；超疏水性；摩擦学性能；耐腐蚀性

作者简介：郭嘉梁，男，1993年生，博士，郑州大学电气与信息工程学院，河南 郑州 450001，E-mail：gsafeg@163.com